



# Thermal–mechanical metamaterial analysis and optimization using an Abaqus plugin

Ewan Fong<sup>1</sup> · Kimmo Koponen<sup>1,2</sup> · Sadik Omairey<sup>3</sup> · Peter Dunning<sup>1</sup>

Received: 1 September 2022 / Accepted: 13 May 2023 / Published online: 17 June 2023  
© The Author(s) 2023

## Abstract

This paper demonstrates how commercial finite-element software and optimization algorithms can be combined to fully explore the design space of thermal–mechanical metamaterials to reveal trends and new insight. This is achieved by developing an Abaqus plugin (EasyPBC) that automates the application of periodic boundary conditions and computes effective elastic and thermal expansion properties for 2D and 3D problems. Abaqus is then linked to an optimizer to fully explore the design space and optimal trade-off between thermal and mechanical properties for two example metamaterials. The first example is a auxetic 2D star-shaped metamaterial, where the proposed approach is used to create a design envelope for Poisson's ratio and thermal expansion coefficient by solving a series of constrained optimization problems. The second example is a 3D metamaterial based on an octet truss, with additional members to expand the design space. A multi-objective optimization problem is solved to find the optimal trade-off between Young's modulus and thermal expansion coefficient in a prescribed direction. The results of both examples expand our knowledge about the range of properties for these metamaterials, and designs for optimal trade-off between thermal and mechanical properties.

**Keywords** Metamaterial · Auxetic · Non-positive thermal expansion coefficient · Optimization · Periodic homogenization

## 1 Introduction

Metamaterials are engineered materials that have properties not usually found in nature, primarily due to their structure, rather than chemical composition. Early metamaterial research focused on electromagnetic properties, such as materials with negative permittivity and permeability [1]. More recently, interest has spread into other areas including acoustic [2], mechanical [3–5] and thermal properties [6]. This paper is focused on thermal–mechanical metamaterials that exhibit extreme stiffness and thermal expansion properties.

Auxetic materials are a type of metamaterial with an extreme stiffness property, as they have a negative Poisson's ratio. Their development can be traced back to the pioneering work of Lakes on auxetic foams [7]. Many auxetic materials have since been developed, including lattice structures, rotating polygons, chiral structures, crumpled and perforated sheets [4]. Auxetic materials have been shown to have several useful engineering properties, such as improved indentation resistance, energy absorption and fracture resistance [3–5]. Thus, they have found many practical application areas, including medical devices (e.g., stents), protective devices and smart sensors and filters [4, 5].

Metamaterials with a non-positive coefficient of thermal expansion (CTE) either contract with temperature increase (negative CTE) or remain the same size (zero CTE). These properties can be achieved by designing metamaterials composed of two materials with different CTE values and some void space [8, 9]. Non-positive CTE metamaterials have potential use in temperature-sensitive applications, such as sensors, thermal–mechanical actuators and structures subject to thermal shock [3].

Metamaterials are often designed for a single novel property, but some studies aim to exploit the idea further

✉ Peter Dunning  
peter.dunning@abdn.ac.uk

<sup>1</sup> School of Engineering, University of Aberdeen, King's College, Aberdeen AB24 3UE, UK

<sup>2</sup> Department of Mechanical Engineering, Colorado School of Mines, Golden 80401, CO, USA

<sup>3</sup> Brunel Composites Centre, College of Engineering, Design and Physical Sciences, Brunel University London, London, UK

by designing multifunctional metamaterials that have two or more novel properties. For example, there have been several recent studies designing metamaterials for both negative Poisson's ratio and non-positive CTE [10]. Grima et al. [11] proposed a 2D lattice metamaterial composed of connected triangles, where one side of a triangle is made from a material with different CTE than the other two sides. Ha et al. [12] showed experimentally that a bimetallic auxetic chiral metamaterial can also have negative CTE and that Poisson's ratio and CTE are independent. Ai and Gao [13] proposed four bi-material lattice metamaterials based on 2D star-shaped re-entrant structures. These were analyzed using finite-element analysis (FEA) and periodic homogenization, showing one of the proposed designs obtained both auxetic behavior and non-positive CTE. This idea was extended by combining several 2D square star-shaped structures with negative thermal expansion coefficient in different patterns [14] and to design 3D metamaterial lattices [15]. Raminhos et al. [16] experimentally investigated one of the metamaterial designs of Ai and Gao [13] (with polymeric materials, instead of metallic) and confirmed the auxetic and negative CTE properties.

Furthermore, designing for one extreme property may lead to unacceptable performance in other properties. For example, metamaterial structures for negative Poisson's ratio or non-zero CTE usually rely on deformation mechanisms that lead to low stiffness (low Young's modulus) [17], which may limit their application. Therefore, some studies aim to achieve a certain novel property, while maximizing other properties. For example, Steeves et al. [18] proposed 2D and 3D lattice structures with low, or zero CTE, but high stiffness. This was achieved using lattice structures with stretch dominated deformation mechanisms (rather than bending dominated). Peng and Bargmann [17] recently proposed a hybrid-honeycomb structure that had auxetic and negative CTE properties, with higher stiffness, compared to some other metamaterial concepts. Other studies also showed improved stiffness of 3D lattice thermal–mechanical metamaterials [19, 20].

The studies mentioned above that propose and design thermal–mechanical metamaterials use parametric studies to explore the potential range of properties, where one or two variables are changed at a time, while others remain constant [13–15, 17, 19]. Thus, the parametric study approach does not fully explore the design space, or the full range of potential properties. Optimization methods can efficiently explore the full design space of a metamaterial concept by allowing all design variables to change simultaneously to meet certain objectives and constraints. Thus, optimization methods can determine the full extent that a metamaterial concept expands the material property space, and can help identify trends and design rules.

The purpose of this paper is not to create fundamentally new metamaterial concepts or optimization algorithms, but to show how numerical simulation and optimization tools can be combined to rapidly explore the design space of a metamaterial concept, so that its full potential can be exploited. To achieve this, an existing Abaqus plugin for periodic homogenization (EasyPBC [21]) is extended to compute thermal expansion coefficients. Two examples are then shown, where the plugin is combined with an optimization algorithm to design and optimize thermal–mechanical metamaterials. The results demonstrate how this approach can extend our knowledge of metamaterials and find the optimal trade-off between thermal and mechanical properties.

## 2 Periodic homogenization with Abaqus

The finite-element method (FEM) and periodic homogenization are used to compute the properties of thermal–mechanical metamaterials. This numerical simulation approach is flexible and general, as it can analyze metamaterials of arbitrary complexity, which may be difficult using analytical models. Thus, the use of finite-element analysis (FEA) is becoming popular to analyze new metamaterial concepts, e.g., [13, 15, 17]. However, applying appropriate periodic boundary conditions may not be straight-forward, especially for complex metamaterials, leading to a time consuming process. Thus, we developed a plugin for Abaqus called EasyPBC that automatically creates periodic boundary conditions for 2D and 3D models [21]. The original plugin can also compute effective elastic properties. In this work, we extend the plugin to compute effective CTE values of 2D and 3D materials.

In EasyPBC, periodic boundary conditions are applied using constraint equations. The algorithm is detailed in [21] and briefly summarized here. First, the user creates a FE model of the representative volume element (RVE) that must be cuboid in shape (or rectangular in 2D), with faces (or edges) aligned with the global coordinate axes. The plugin then identifies nodes on each face, sorted into sets. Pairs of nodes on opposite faces are found by looking at their coordinates. Finally, constraint equations are applied to each pair of nodes to model the periodic boundary conditions. For example, when computing Young's moduli, the following constraint equations are applied:

$$\begin{aligned}
 u_{\text{right}} - u_{\text{left}} &= \Delta^x \\
 v_{\text{right}} - v_{\text{left}} &= 0 \\
 w_{\text{right}} - w_{\text{left}} &= 0 \\
 u_{\text{front}} - u_{\text{back}} &= 0 \\
 v_{\text{front}} - v_{\text{back}} &= \Delta^y \\
 w_{\text{front}} - w_{\text{back}} &= 0 \\
 u_{\text{top}} - u_{\text{bottom}} &= 0 \\
 v_{\text{top}} - v_{\text{bottom}} &= 0 \\
 w_{\text{top}} - w_{\text{bottom}} &= \Delta^z
 \end{aligned}
 \tag{1}$$

where  $u$ ,  $v$  and  $w$  are displacements in the  $x$ ,  $y$  and  $z$ -directions, respectively. The left and right faces are perpendicular to the  $x$ -axis, front and back faces perpendicular to the  $y$ -axis, and top and bottom faces perpendicular to the  $z$ -axis. Therefore,  $u_{\text{right}}$  is the  $u$  displacement of a node on the right face, which is linked to the  $u$  displacement of the opposite node on the left face,  $u_{\text{left}}$ . The values  $\Delta^x$ ,  $\Delta^y$  and  $\Delta^z$  are displacements of auxiliary reference points, which are used to apply and measure strain, or apply further constraints. For example, to compute Young’s modulus in the  $x$ -direction,  $\Delta^y$  and  $\Delta^z$  are set to zero and  $\Delta^x$  set to 1. Using applied displacements to determine effective properties is easier to implement in Abaqus compared with directly solving the asymptotic homogenization equations, which requires information about the element formulation [22]. Further details, and the constraint equations for computing shear moduli, can be found in [21].

In this work, the plugin is extended to calculate CTE values. This is achieved by prescribing a temperature change,  $\Delta T$ , to the whole model. The values of  $\Delta^x$ ,  $\Delta^y$  and  $\Delta^z$  in Eq. 1 are free and determined by the solver. These are then used to compute CTE values:

$$\begin{aligned}
 \alpha_x &= \Delta^x / (L_x \Delta T) \\
 \alpha_y &= \Delta^y / (L_y \Delta T) \\
 \alpha_z &= \Delta^z / (L_z \Delta T)
 \end{aligned}
 \tag{2}$$

where  $L_x$  is the length of the RVE in the  $x$ -direction. The extended plugin for determining homogenized properties is now used to optimize and explore the design space of thermal–mechanical metamaterials.

### 3 Example 1—design envelope generation

When a new metamaterial is proposed it is useful to explore the design space to determine its full potential and compare properties with other metamaterials. However, many studies that propose, or design new metamaterial only use parametric studies to explore the potential range of properties, e.g.,

[13–15, 23], where only one, or two variables are changed at a time, while others remain constant. Thus, this parametric approach does not explore the full range of potential properties. Optimization methods can better explore the design space by simultaneously changing all design variables. In this example, we show how the FE-based plugin for periodic homogenization described above can be combined with an optimization algorithm to explore the full range of possible novel properties of a thermal–mechanical metamaterial. Thus, a design envelope of these novel properties is generated in an efficient and automated way.

### 3.1 Methodology

The design envelope for a 2D thermal–mechanical metamaterial is generated by solving a series of single objective optimization problems with different constraints. To begin the process, unconstrained optimization problems are solved to maximize, or minimize the properties that are to be explored. Once the maximum and minimum values of the properties are established, a series of constrained optimization problems are solved to find the boundaries of the design envelope.

In this example, we aim to explore the range of Poisson’s ratio and CTE of a thermal–mechanical metamaterial. Note that in practice we optimize the normalized CTE (NCTE), where the CTE value is normalized by the CTE of one of the constituent materials (in the example below we use Aluminum,  $\alpha = 23 \times 10^{-6}/^\circ\text{C}$ ). First, four problems are solved: maximize Poisson’s ratio (Max  $\nu$ ), minimize Poisson’s ratio (Min  $\nu$ ), maximize NCTE (Max NCTE), and minimize NCTE (Min NCTE), with only side constraints on the design variables (see Sect. 3.2). These upper and lower limits for the properties are then used to solve a series of optimization problems, where one of the properties is minimized (to explore the novel properties of negative Poisson’s ratio and negative CTE), with upper, or lower bound constraints on the other property. Where  $\nu_L$  is a lower limit on Poisson’s ratio,  $\text{NCTE}_L$  is a lower limit on NCTE, and  $\text{NCTE}_U$  is an upper limit on NCTE.

All optimization problems are solved using an Augmented Lagrangian Particle Swarm Optimizer (ALPSO) [24] implemented in the package pyOpt [25], with all options set to default.

### 3.2 2D star-shaped metamaterial

The metamaterial considered in this example is based on a design proposed by Ai and Gao [13]. Their study considered a set of four different bi-material lattice structures with the goal of creating a metamaterial that can exhibit both non-positive CTE and negative Poisson’s ratio. One of the lattice structures (Fig. 1) provided promising results, where both

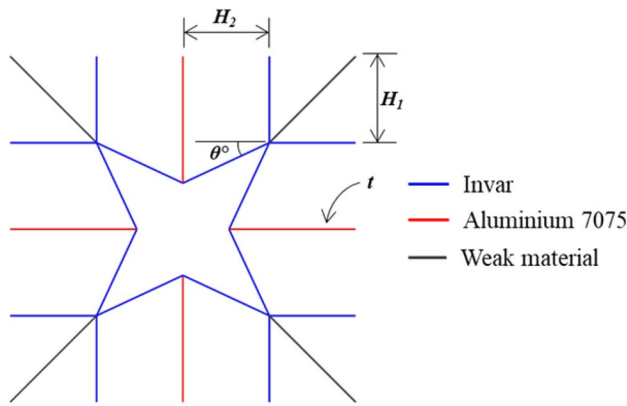


**Fig. 1** Star-shaped lattice metamaterial

**Table 1** Material properties for the star-shaped metamaterial

Material	$E$ (GPa)	$\nu$	CTE $\alpha$ ( $10^{-6}$ / °C)	Temperature (°C)
Aluminum	71	0.33	23.0	20
	66		24.3	200
Invar	144	0.29	1.1	20
	135		2.5	200

negative Poisson's Ratio and non-positive CTE values were shown. In addition, their study considered three constituent materials: Aluminum Alloy, Steel and Invar, resulting in three different material pairings. However, it was found that the Aluminum–Invar pair led to a metamaterial exhibiting non-positive CTE over a wide range of design parameters. Thus, the Aluminum–Invar material pairing is chosen in this example to provide the optimizer with a larger design space for both non-positive CTE along with negative Poisson's Ratio. Properties of the constituent materials are summarized in Table 1. Note that the lattice structure is square symmetric, so  $\nu_{12} = \nu_{21} = \nu$ , and  $\alpha_1 = \alpha_2 = \alpha$ .

Beam elements are used for the FE model, as the members in the lattice are long and thin (beam elements were also used by Ai and Gao [13]). Two-node Timoshenko beams (element type B31) are used. Meshing is automatic, with an approximate element length (global seed size) set to 0.085 times the RVE edge length, which creates meshes with between 150 and 200 elements.

The lattice structure used in this example has one difference to the one used by Ai and Gao [13], as extra beams in the corners are incorporated to make it compatible with EasyPBC, where corner nodes are required to accurately determine its size. Note this could be avoided by modifying the plugin by hard coding the RVE size, but we wanted to demonstrate the use of the plugin without modification. To ensure these beams have negligible effect on computed

properties, a fictitious “weak material” is used. The weak material has a low Young's modulus of  $E = 1$  kPa and a CTE similar to Invar and Aluminum ( $\alpha = 10^{-6}/^\circ\text{C}$ ). The modified structure is validated by comparing the material properties calculated in this study to those reported by Ai and Gao [13], showing negligible difference.

The design variables for optimization are lengths  $H_1$  and  $H_2$ , and angle  $\theta$  in Fig. 1, plus the in-plane thickness,  $t$ , of the beams. Note that the out-of-plane thickness of the beams does not affect homogenized properties of the 2D metamaterial. The limits on design variables are:  $5 \leq H_1 \leq 100$ ,  $5 \leq H_2 \leq 100$ ,  $5^\circ \leq \theta \leq 40^\circ$ , and  $0.5 \leq t \leq 5$ . To compute CTE, a temperature change from 0 to 200 °C is applied.

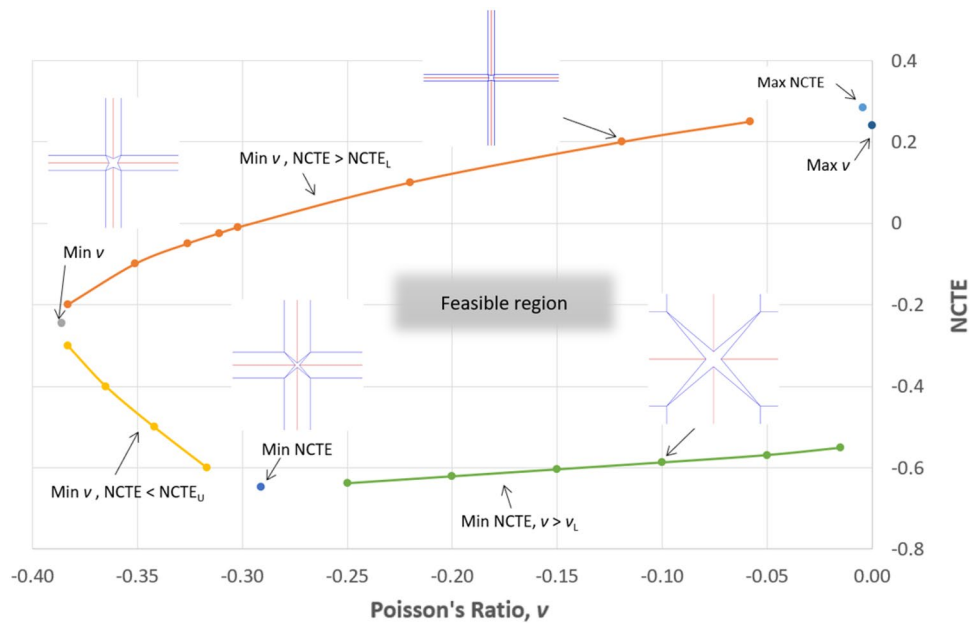
### 3.3 Results

Figure 2 shows the design envelope created by the method described above for the 2D star-shaped metamaterial. Design variables for optimum designs are summarized in Appendix A.

The results show a wide range of solutions for both negative Poisson's Ratio and negative NCTE; covering ranges of:  $-0.386 \leq \nu$ , and  $-0.647 \leq \text{NCTE}$ , or  $-14.9 \times 10^{-6}/^\circ\text{C} \leq \alpha$ . The approximate range of these properties reported by Ai and Gao [13] using parametric studies are smaller:  $-0.19 \leq \nu$  and  $-0.60 \leq \text{NCTE}$ , or  $-13.8 \times 10^{-6}/^\circ\text{C} \leq \alpha$ . This demonstrates how optimization can be used to explore the full range of potential properties of a thermal–mechanical metamaterial concept. The resulting design envelope can then be used as a guide, and metamaterial properties can be tailored towards specific applications by using an optimizer to minimize, maximize and possibly constrain properties to achieve the desired behavior.

Further insight is gained by examining the variation of optimal design parameters along the edge of the design envelope. The full set of results is summarized in Appendix A. For example, starting at the maximum NCTE point and moving anti-clockwise around the edge of the design envelope, the ratio of  $H_1/H_2$  starts at its maximum possible value and decreases to its minimum possible value. The angle,  $\theta$ , also increases anti-clockwise, until it reaches its maximum value of  $40^\circ$  at the minimum NCTE point, thereafter it remains at  $40^\circ$ . These trends correspond to a general reduction in CTE, where negative CTE is achieved by exploiting the central star shape. It is observed that when the ratio of  $H_1/H_2$  is large, then central star shape is small, relative to RVE size, which reduces its influence on CTE properties as the displacement within the central star shape is small, compared with the displacement of the vertical and horizontal beams. For Poisson's ratio, it is observed that different designs can achieve the same auxetic behavior. Designs with larger, positive CTE values achieve auxetic behavior with smaller  $\theta$  and a larger ratio of  $H_1/H_2$ . Whereas designs with lower,

**Fig. 2** Design envelope for the 2D star-shaped lattice meta-material.  $\nu_L$  is a lower limit on Poisson’s ratio,  $NCTE_L$  is a lower limit on NCTE, and  $NCTE_U$  is an upper limit on NCTE



**Table 2** Comparison of computed effective properties using beam element and solid element finite-element modeling

Design	Beam elements		2D continuum elements	
	$\nu$	NCTE	$\nu$	NCTE
Max $\nu$	0.0003	0.2410	0.0538	0.2940
Max NCTE	-0.0044	0.2850	0.0457	0.3010
Min $\nu$ , NCTE > 0.25	-0.0580	0.2500	-0.0505	0.2478
Min $\nu$ , NCTE > 0.20	-0.1190	0.2000	-0.1318	0.1895
Min $\nu$ , NCTE > 0.10	-0.2200	0.1000	-0.2381	0.0820
Max $\nu$ , NCTE < 0.0	-0.0150	-0.5510	-0.00862	-0.555

negative CTE achieve auxetic behavior with bigger angles and smaller ratios of  $H_1/H_2$ . This demonstrates the utility of optimization when analyzing metamaterial properties, as these trends rely on the simultaneous variation of multiple parameters.

The results obtained in Fig. 2 are obtained using beam finite elements to be consistent with Ai and Gao [13]. This approximates the behavior of the metamaterial, especially around the joints, which is reasonable if members are thin. To validate the results, some designs with the biggest beam thickness values are reanalyzed using 2D quadratic continuum elements. Table 2 shows the comparison of effective material properties, where most values from the beam model are within 10% of those calculated using continuum elements. The exception is when Poisson’s ratio is near zero, where the absolute error is within 0.06. Therefore, we conclude that if the entire design envelope in Fig. 2 is

recomputed using solid elements, then the shape would be the same, but the exact values would alter slightly.

## 4 Example 2—multi-objective optimization

When materials are subject to both loading and temperature increase, the total deformation depends on the material stiffness and CTE. In many applications, it is important to minimize deformation, for example the radial expansion of a turbine blade during operation [26]. Thus, there is interest in finding the optimal trade-off between high stiffness and low CTE for thermal–mechanical metamaterials.

### 4.1 Methodology

The optimal trade-off between stiffness and CTE of a 3D lattice-type thermal–mechanical metamaterial is explored by generating the Pareto front using a multi-objective Genetic Algorithm (GA). We assume that deformation in a certain direction should be minimized and therefore the first objective is to maximize the Young’s modulus in that direction,  $E_y$  (the y-direction is chosen arbitrarily). The second objective is to minimize the square of the CTE in the same direction,  $\alpha_y^2$ , to achieve close to zero CTE. Young’s modulus and CTE are computed using the EasyPBC Abaqus plugin (as detailed in Sect. 2). The multi-objective problem is solved using the GA implemented in Matlab, which is based on NSGA-II [27], modified to handle integer design variables [28], so that material choice can be used as a design variable.

## 4.2 Extended 3D octet truss metamaterial

The metamaterial optimized in this example is based on a 3D octet truss [29], with additional members added to enlarge the design space and potentially find novel metamaterials. The base unit cell is shown in Fig. 3. The truss is split into 5 groups of members, as shown by the different colors in Fig. 3. This reduces the number of design variables, allowing the use of a non-gradient-based optimization method. Note that the original octet truss is composed of just the blue and red members.

The length of the unit cell in the  $x$ -direction,  $L_x$  is set to 1, and the length in the  $y$ -direction,  $L_y$ , can be chosen by the optimizer to change the skew angles of the octet truss. The length in the  $z$ -direction,  $L_z$ , is set so that the volume of the unit cell is 1 (i.e.,  $L_z = 1/L_y$ ). Note that due to the asymptotic periodic homogenization assumptions, the homogenized properties are independent of the length scale used, and thus no units are given for length variables in the unit cell.

The truss members are assumed hollow circular, but the lower bound for the inner radius,  $r_i$  is set to zero, allowing the optimizer to choose solid circular members. The upper bound for the outer radius,  $r_o$ , is set to 0.13, which results in a maximum volume fraction of approximately 40% for the unit cell. To avoid impossible geometry, where  $r_i > r_o$ , constraints are added to the optimization problem to ensure the minimum thickness of any member is at least  $10^{-3}$ .

To tune the CTE of a metamaterial, it must be made from at least 2 different materials, with different CTE values. In this study, members can be made from a titanium alloy (Ti-6242), or a stainless steel (AISI 321), with properties summarized in Table 3. Properties are obtained from [30, 31], where temperature dependence for  $E$  and  $\alpha$  is included if data are available.

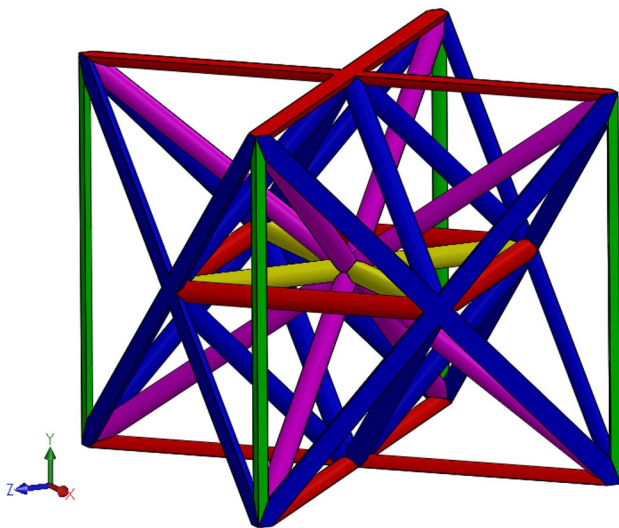


Fig. 3 Extended octet truss metamaterial

To compute CTE, a temperature change from 0 to 500 °C is applied. The optimizer can also choose a void material, with all properties close to zero ( $10^{-15}$ ). This enables some limited topology optimization of the metamaterial, as assigning void material effectively removes a set of members from the design. Material choice is a discrete design variable and is coded as an integer variable, with 0 = void, 1 = Ti-6242, and 2 = AISI 321. A constraint is added such that the sum of the material integer variables must be at least 3 to avoid fully void designs. The full set of design variables is summarized in Table 4.

The multi-objective optimization problem is then:

$$\begin{aligned} \min_{\mathbf{x}} \left( 10^{10} \alpha_y^2 \right), \max_{\mathbf{x}} \left( 10^{-10} E_y \right) \\ \text{Subject to : } \sum_{j=1}^5 M_j \geq 3 \\ r_{0j} - r_{ij} \geq 10^{-3}, j = [1, 5] \\ \mathbf{x}_{\min} \leq \mathbf{x} \leq \mathbf{x}_{\max} \end{aligned} \quad (3)$$

where  $\mathbf{x}$  is the set of design variables, as defined in Table 4, subscript  $j$  refers to the set of members, as defined in Fig. 3 (1 = blue, 2 = red, 3 = yellow, 4 = green, 5 = purple).

Table 3 Material properties for extended octet truss optimization

Material property	Temperature (°C)	Ti-6242	AISI 321
Young's modulus, $E$ (GPa)	0	115.0	195.0
	500	87.0	158.4
Poisson's ratio, $\nu$	–	0.36	0.27
Density, $\rho$ (kg/m <sup>3</sup> )	–	4540	7950
CTE, $\alpha$ ( $10^{-6}/^\circ\text{C}$ )	20	6.55	18.6
	77	7.52	
	133	8.19	
	190	8.65	
	247	8.96	
	303	9.2	
	360	9.38	
	417	9.54	
	473	9.67	
	530	9.74	

Table 4 Design variables for extended octet truss

Design variable	Type	Minimum	Maximum
Outer radius, $r_o$	Continuous	$10^{-4}$	0.13
Inner radius, $r_i$	Continuous	0	0.08
Material, $M$	Integer	0	2
Unit cell length in $y$ , $L_y$	Continuous	0.67	1.5

Scaling is used to make the two objectives approximately equal in magnitude.

### 4.3 FE modeling and validation

To accurately compute effective properties of the metamaterial it is recommended to use 3D continuum elements, as these can accurately represent the geometry, especially the joints where multiple members overlap. However, using 3D continuum elements leads to long computation times that prohibits the use of multi-objective GA optimization. In addition, robust, automated 3D meshing of the joints is not straight-forward, which also makes this approach challenging to use within an optimization algorithm. Therefore, a beam element model is used to reduce computational time and simplify the automated meshing process.

To validate the beam element approach, we compare the computed effective properties of an octet truss metamaterial [32] modeled using Timoshenko beam elements (B31 in Abaqus), with those computed using quadratic tetrahedral 3D continuum elements (C3D10). For all beam element models, 6 elements per member are used, as using more elements changed effective properties by less than 1%. Members that lie on the RVE face, or edge, are only half, or quarter, inside the RVE. This is easily accounted for when using 3D elements, as the geometry can be modeled exactly, but some modification is required when using beam elements. All beam elements used in this work have circular (or hollow circular) cross-sections. Members that lie along an RVE face are modified by scaling their radius such that their cross-sectional area is a half (as only half the member is inside the RVE). A similar modification is made to members that lie along RVE edges, where the radius is scaled such that the cross-sectional area is one quarter.

This approach is accurate for modeling the tensile and compressive behavior of members, as axial stiffness is directly proportional to cross-sectional area, but may not be accurate for bending behavior. However, it is known that the octet truss is a stretching dominated metamaterial, where the loading on members is predominantly tension or compression [32], so this is not thought to introduce significant error. However, representative optimal results are reanalyzed using 3D continuum elements in Sect. 4.4 to validate this.

Effective properties are computed for an octet truss with increasing relative density, which is controlled by increasing member radius, where all members have the same radius. Relative density is defined as the actual density of the metamaterial divided by the density of the constituent materials in the ratio they are used [32]. For stiffness analysis, the whole octet structure is made of Aluminum, but for the CTE analysis, the members along the RVE faces are made from titanium. The relative percentage error between the beam and 3D element models is shown in Fig. 4, which shows

that the error increases as relative density increases. This is mainly due to the increased overlap in the joint regions when member radius is increased, which is not accurately captured by the beam element model. However, the beam model is able to accurately capture the trend in material properties. When comparing computational cost, on our computer, the beam element model is approximately 100 times faster than the 3D element model. In conclusion, the beam element model is suitable for the purpose of optimization. Although the error increases with relative density, the trend in properties is captured, and the computational cost is significantly lower. However, it is recommended to recompute effective properties of optimal designs using 3D elements to obtain a more accurate prediction.

### 4.4 Results

The first optimization run uses all design variables listed in Table 4. The GA optimizer is run with a population of 70 for 55 generations. The analysis of the results shows a trend in material choices along the Pareto front, as the material for member set 1 (blue in Fig. 3) is almost always titanium, whereas the material for set 2 (red in Fig. 3) tends to be AISI 321 steel (note that sets 1 and 2 are the original octet truss). This combination helps reduce CTE in the  $y$ -direction, as the higher CTE material (AISI 321) is in the  $x$ - $z$  plane, which when it expands reduces strain in the  $y$ -direction via the lattice structure and lower CTE material (Ti-6242).

A second run is completed, where the optimizer is forced to use titanium and steel for member sets 1 and 2, respectively. Using the same population size and number of generations, the Pareto front for this restricted problem improves, as shown in Fig. 5. This can be explained by the optimizer having a smaller design space to explore when material choice is restricted, so it is more likely to find better designs (closer to the true Pareto front) with

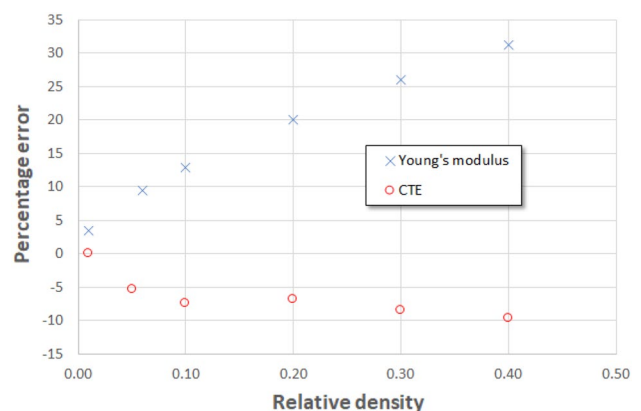
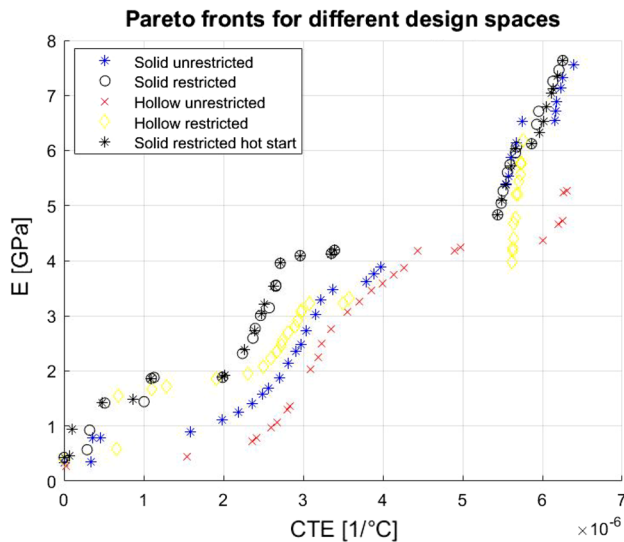


Fig. 4 Relative error between beam and 3D continuum element models



**Fig. 5** Pareto fronts from optimization runs with different restrictions on design variables. ‘Restricted’ means that the material of set 1 and 2 are set to titanium and steel, respectively

the computational resources available (population size and number of generations). It is reasonable to assume that if the original problem was given a large enough initial population and number of generations, it would eventually reach the same results as the restricted run. However, this could take a significant amount of time, which is why it is useful to restrict the design space based on trends observed in the initial results.

Next, to investigate the potential benefit of hollow members, the problem is further restricted to use solid members only ( $r_i = 0$ ) and the Pareto fronts are compared. The first run with solid members does not restrict material choice. As expected, the same trend occurs, with the material for set 1 tending to be titanium and set 2 being steel. Therefore, a further run with restricted material choice and solid members is conducted. As before, the Pareto front improves after forcing the optimizer to use titanium and steel for sets 1 and 2, respectively (see Fig. 5).

To see if the Pareto front can be improved further, a fifth run is completed using a ‘hot start’, where the results from the solid restricted run are used as part of the initial population. This allows the optimizer to start with a strong population, which helps it find even better designs. However, as Fig. 5 shows, the Pareto front from the ‘hot start’ does not significantly improve from the initial population. This gives us confidence that a set of designs close to the true Pareto front is found. For clarity, the ‘hot start’ Pareto front is shown in Fig. 6, where 3 distinct regions can be seen, with clear gaps between each region. Note that the different colors in Fig. 6 are used to highlight the 3 regions, but all points belong to the Pareto front. It is not clear why

there are gaps, but it could be that the optimizer has difficulty finding solutions in these gaps, as there seem to be parts of the Pareto front with very similar stiffness values, but different CTE values. Furthermore, there is no clear trend in the designs within each region, which is interesting and suggests that different designs can achieve similar (or even the same) stiffness and CTE values in the y-direction.

All results show that Young’s modulus and CTE in the optimized direction are proportional, where modulus increases as CTE increases. However, to minimize deformation under loading and temperature increase, a material with high modulus and low CTE is desirable. Therefore, the best choice for a certain application will depend on the relative influence of loading and temperature increase on deformation. For example, if temperature increase is more influential, then a material with smaller CTE should be chosen. This demonstrates the utility of having the optimal trade-off between these properties available in the form of a Pareto front.

Three designs from the Pareto front are chosen for further investigation, which are indicated by the circles in Fig. 6. The parameters for each design are summarized in Table 5, which shows some similarities in the chosen designs. The outer radius is relatively large for both member set 1 and 2, suggesting these play a dominant role in achieving optimal balance between high stiffness and low CTE. Similarly, the material for sets 4 and 5 is the same, i.e., Ti-6242. This suggests that the material choice for sets 4 and 5 could also be restricted, but other designs on the hot start Pareto front show variation in these material choices, which is why they are not restricted during optimization.

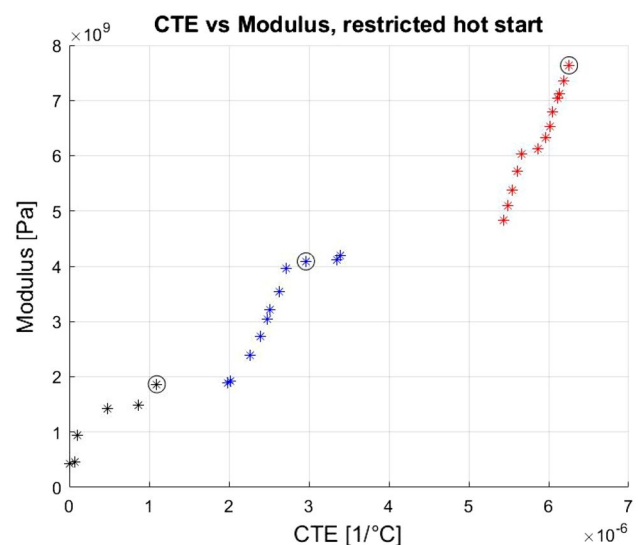


**Fig. 6** Pareto front from the ‘hot start’ using solid members are restricted material choice



**Table 5** Design parameters for three designs on the Pareto front (identified by circles in Fig. 6)

Design variable		Design 1 (black)	Design 2 (blue)	Design 3 (red)
Outer radius	$r_{0,1}$	0.0916	0.1212	0.119
	$r_{0,2}$	0.0997	0.0966	0.0972
	$r_{0,3}$	0.012	0.058	0.1166
	$r_{0,4}$	0.0628	0.0933	0.0157
	$r_{0,5}$	0.0726	0.0173	0.0907
Material choice	$M_1$	Ti-6242	Ti-6242	Ti-6242
	$M_2$	AISI 321	AISI 321	AISI 321
	$M_3$	Ti-6242	Void	AISI 321
	$M_4$	Ti-6242	Ti-6242	Ti-6242
	$M_5$	Ti-6242	Ti-6242	Ti-6242
RVE side length	$L_y$	0.9385	1.1124	1.3036

Effective material properties for the three designs are computed using both beam and 3D continuum elements, and summarized in Table 6. All designs show significant anisotropic properties, which is expected because the optimization problem did not enforce cubic symmetry, and only Young’s modulus and CTE in the  $y$ -direction are optimized. Comparing results from the beam and 3D element models, the maximum error in Young’s modulus is approximately 20%, and CTE approximately  $-17\%$  (although most errors are below 10%). This is within the range expected from Fig. 4, and demonstrates why post-optimization analysis with 3D continuum elements is needed to more accurately estimate effective metamaterial properties.

**Table 6** Effective material properties for three designs on the Pareto front (identified by circles in Fig. 6)

Model	Material property	Design 1	Design 2	Design 3
Beam elements	$E_x$ (GPa)	1.85	2.63	5.28
	$E_y$ (GPa)	1.86	4.12	7.57
	$E_z$ (GPa)	2.36	1.73	2.67
	$\alpha_x$ ( $10^{-6}/^\circ\text{C}$ )	18.17	17.19	17.88
	$\alpha_y$ ( $10^{-6}/^\circ\text{C}$ )	1.09	2.95	6.25
	$\alpha_z$ ( $10^{-6}/^\circ\text{C}$ )	17.32	18.91	19.06
	$\rho$ ( $\text{kg}/\text{m}^3$ )	813	1143	1130
3D continuum elements	$E_x$ (GPa)	2.08	3.21	5.73
	$E_y$ (GPa)	2.09	4.58	7.68
	$E_z$ (GPa)	2.63	2.15	3.11
	$\alpha_x$ ( $10^{-6}/^\circ\text{C}$ )	17.99	16.99	17.70
	$\alpha_y$ ( $10^{-6}/^\circ\text{C}$ )	1.31	3.32	6.38
	$\alpha_z$ ( $10^{-6}/^\circ\text{C}$ )	17.20	18.41	18.91
	$\rho$ ( $\text{kg}/\text{m}^3$ )	741	994	971

Design 1 (black circle in Fig. 6) is shown in Fig. 7 and discussed in more detail. This configuration has higher CTE materials only in the  $x$ - $z$  plane, and works in a similar way as the triangular shape proposed by Wei et al. [33]. When temperature increases, the red members (AISI 321) expand in  $x$  and  $z$ -directions, and the blue (Ti-6242) diagonal and vertical members expand less. The combined effect is that the expansion in the  $y$ -direction is significantly smaller than if the whole metamaterial was made from Ti-6242.

### 5 Conclusions

This paper combines a commercial finite-element package with optimization methods to explore the design space and optimal design of thermal–mechanical metamaterials. A plugin for Abaqus that automatically applies periodic boundary conditions and compute effective elastic properties (EasyPBC) is extended to compute effective thermal expansion coefficients for 2D and 3D problems.

The proposed approach is demonstrated using two example problems. The first problem uses a particle swarm optimizer to solve a series of constrained problem that generate the design envelope of Poisson’s ratio and CTE for a 2D star-shaped lattice metamaterial. The results extend the range of possible auxetic and negative CTE compared with a previous study that used parametric studies.

The second example uses a multi-objective genetic algorithm to find the optimal trade-off between Young’s modulus and CTE in a particular direction for an extended octet truss. The results show that the best material choice for lattice members from the original octet truss are to use the higher CTE material for members orthogonal to the

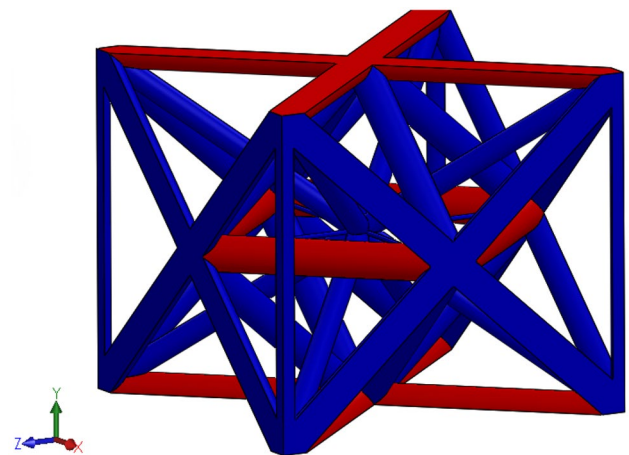


**Fig. 7** Design 1 from the Pareto front (black circle in Fig. 6). Blue members are Ti-6242 and red members are AISI 321

direction of interest, and lower CTE material for remaining members, which helps reduce CTE in the direction of interest. However, there was no trend for other parameters along the Pareto front, suggesting that different designs can achieve similar (or the same) stiffness and CTE in the direction of interest. In addition, the results show little benefit of using hollow members, compared with solid members, because the deformation mechanisms of the lattice result in members being strained predominantly in tension, or compression.

Manufacture of the multiple metal lattice structures explored in this work is challenging, but possible. Conventional manufacturing methods such as investment casting, expanded metal sheet, metallic wire assembly, and snap fit methods can be adopted to manufacture multiple metal lattices (see [32]—for example). In addition, some additive manufacturing methods can also be utilized to produce multiple metal parts [34].

## Appendix A: Optimization results for star-shaped lattice metamaterial (Sect. 2)

See Table 7.

**Table 7** Full results for the design envelope in Fig. 2

	$H_1/H_2$	$\theta$ (°)	$t/L$	$\nu$	NCTE
Max $\nu$	9.54	39.56	0.04497	0.000	0.241
Max NCTE	20.00	5.00	0.0238	-0.004	0.285
Min $\nu$	20.00	14.62	0.00652	-0.058	0.250
NCTE > NCTE <sub>L</sub>	20.00	15.00	0.00391	-0.119	0.200
	19.70	16.58	0.00241	-0.220	0.100
	14.18	16.84	0.00234	-0.302	-0.010
	13.50	16.96	0.00233	-0.311	-0.025
	12.41	17.19	0.00231	-0.326	-0.050
	10.24	17.92	0.00228	-0.351	-0.100
	7.41	21.20	0.00220	-0.383	-0.200
Min $\nu$	7.50	23.85	0.00220	-0.386	-0.246
Min $\nu$	7.15	26.51	0.00219	-0.383	-0.300
NCTE < NCTE <sub>U</sub>	6.80	31.12	0.00218	-0.365	-0.400
	6.62	35.24	0.00217	-0.342	-0.500
	6.49	38.90	0.00217	-0.317	-0.600
Min NCTE	4.00	40.00	0.00200	-0.291	-0.647
Min NCTE	2.16	40.00	0.00171	-0.250	-0.638
$\nu > \nu_L$	1.20	40.00	0.00137	-0.200	-0.621
	0.70	40.00	0.00147	-0.150	-0.604
	0.38	40.00	0.00181	-0.100	-0.587
	0.16	40.00	0.00216	-0.050	-0.569
	0.05	40.00	0.02381	-0.015	-0.551

**Funding** No funding was received for conducting this study.

## Declarations

**Conflict of interest** The authors have no competing interests to declare that are relevant to the content of this article.

**Open Access** This article is licensed under a Creative Commons Attribution 4.0 International License, which permits use, sharing, adaptation, distribution and reproduction in any medium or format, as long as you give appropriate credit to the original author(s) and the source, provide a link to the Creative Commons licence, and indicate if changes were made. The images or other third party material in this article are included in the article's Creative Commons licence, unless indicated otherwise in a credit line to the material. If material is not included in the article's Creative Commons licence and your intended use is not permitted by statutory regulation or exceeds the permitted use, you will need to obtain permission directly from the copyright holder. To view a copy of this licence, visit <http://creativecommons.org/licenses/by/4.0/>.

## References

- Engheta N, Ziolkowski RW (2006) *Metamaterials: physics and engineering explorations*. Wiley, Hoboken
- Cummer SA, Christensen J, Alù A (2016) Controlling sound with acoustic metamaterials. *Nat Rev Mater* 1(3):1–13
- Huang C, Chen L (2016) Negative Poisson's ratio in modern functional materials. *Adv Mater* 28(37):8079–8096
- Ren X, Das R, Tran P, Ngo TD, Xie YM (2018) Auxetic metamaterials and structures: a review. *Smart Mater Struct* 27(2):023001
- Surjadi JU, Gao L, Du H, Li X, Xiong X, Fang NX, Lu Y (2019) Mechanical metamaterials and their engineering applications. *Adv Eng Mater* 21(3):1800864
- Sklan SR, Li B (2018) Thermal metamaterials: functions and prospects. *Natl Sci Rev* 5(2):138–141
- Lakes R (1987) Foam structures with a negative Poisson's ratio. *Science* 235:1038–1041
- Lakes R (1996) Cellular solid structures with unbounded thermal expansion. *J Mater Sci Lett* 15(6):475–477
- Sigmund O, Torquato S (1996) Composites with extremal thermal expansion coefficients. *Appl Phys Lett* 69(21):3203–3205
- Cardoso JO, Borges JP, Velhinho A (2021) Structural metamaterials with negative mechanical/thermomechanical indices: a review. *Progr Nat Sci Mater Int* 31:801–808
- Grima NJ, Farrugia P-S, Gatt R, Zammit V (2007) Connected triangles exhibiting negative Poisson's ratios and negative thermal expansion. *J Phys Soc Jpn* 76(2):025001
- Ha C-S, Hestekin E, Li J, Plesha M.E, Lakes R.S (2015) Controllable thermal expansion of large magnitude in chiral negative Poisson's ratio lattices. *Phys Status Solidi (B)* 252(7):1431–1434
- Ai L, Gao X-L (2017) Metamaterials with negative Poisson's ratio and non-positive thermal expansion. *Compos Struct* 162:70–84
- Li X, Gao L, Zhou W, Wang Y, Lu Y (2019) Novel 2D metamaterials with negative Poisson's ratio and negative thermal expansion. *Extreme Mech Lett* 30:100498
- Ai L, Gao X-L (2018) Three-dimensional metamaterials with a negative Poisson's ratio and a non-positive coefficient of thermal expansion. *Int J Mech Sci* 135:101–113
- Raminhos J, Borges J, Velhinho A (2019) Development of polymeric anepectic meshes: auxetic metamaterials with negative thermal expansion. *Smart Mater Struct* 28(4):045010

17. Peng X-L, Bargmann S (2021) A novel hybrid-honeycomb structure: enhanced stiffness, tunable auxeticity and negative thermal expansion. *Int J Mech Sci* 190:106021
18. Steeves C.A, e Lucato S.L.d.S, He M, Antinucci E, Hutchinson J.W (2007) Concepts for structurally robust materials that combine low thermal expansion with high stiffness. *J Mech Phys Solids* 55(9):1803–1822
19. Chen Y, Fu M-H (2017) A novel three-dimensional auxetic lattice meta-material with enhanced stiffness. *Smart Mater Struct* 26(10):105029
20. Huang J, Li W, Chen M, Fu M (2021) An auxetic material with negative coefficient of thermal expansion and high stiffness. *Appl Compos Mater* 29:777–802
21. Omairey SL, Dunning PD, Sriramula S (2019) Development of an ABAQUS plugin tool for periodic RVE homogenisation. *Eng Comput* 35(2):567–577
22. Hassani B, Hinton E (1998) A review of homogenization and topology optimization II—analytical and numerical solution of homogenization equations. *Comput Struct* 69(6):719–738
23. Ng CK, Saxena KK, Das R, Flores ES (2017) On the anisotropic and negative thermal expansion from dual-material re-entrant-type cellular metamaterials. *J Mater Sci* 52(2):899–912
24. Jansen PW, Perez RE (2011) Constrained structural design optimization via a parallel augmented Lagrangian particle swarm optimization approach. *Comput Struct* 89(13–14):1352–1366
25. Perez RE, Jansen PW, Martins JR (2012) pyOpt: a python-based object-oriented framework for nonlinear constrained optimization. *Struct Multidiscip Optim* 45(1):101–118
26. Lagow BW (2016) Materials selection in gas turbine engine design and the role of low thermal expansion materials. *JOM* 68(11):2770–2775
27. Deb K, Pratap A, Agarwal S, Meyarivan T (2002) A fast and elitist multiobjective genetic algorithm: NSGA-II. *IEEE Trans Evol Comput* 6(2):182–197
28. MathWorks Support Team (2018) Is it possible to solve a mixed-integer multi-objective optimization problem using global optimization toolbox? <https://uk.mathworks.com/matlabcentral/answers/103369-is-it-possible-to-solve-a-mixed-integer-multi-objective-optimization-problem-using-global-optimizati>. Accessed 18 Apr 2018
29. Deshpande VS, Fleck NA, Ashby MF (2001) Effective properties of the octet-truss lattice material. *J Mech Phys Solids* 49(8):1747–1769
30. US Department of Defense (1998) Military handbook: metallic materials and elements for aerospace vehicle structures, 5th edn. US Department of Defense, Arlington County
31. American Iron and Steel Institute (1979) High-temperature characteristics of stainless steels. Designers' handbook series. Committee of Stainless Steel Producers, American Iron and Steel Institute, USA. [https://nickelinstitute.org/media/1699/high\\_temperature\\_characteristics\\_of\\_stainless\\_steel\\_9004\\_.pdf](https://nickelinstitute.org/media/1699/high_temperature_characteristics_of_stainless_steel_9004_.pdf)
32. Xu H, Pasini D (2016) Structurally efficient three-dimensional metamaterials with controllable thermal expansion. *Sci Rep* 6(1):1–8
33. Wei K, Chen H, Pei Y, Fang D (2016) Planar lattices with tailorable coefficient of thermal expansion and high stiffness based on dual-material triangle unit. *J Mech Phys Solids* 86:173–191
34. Bandyopadhyay A, Zhang Y, Bose S (2020) Recent developments in metal additive manufacturing. *Curr Opin Chem Eng* 28:96–104

**Publisher's Note** Springer Nature remains neutral with regard to jurisdictional claims in published maps and institutional affiliations.